MOUNTAIN-PLAINS CONSORTIUM

MPC 22-455 | Y. J. Kim

COMPOSITE REPAIR FOR CONCRETE BRIDGES SUBJECTED TO ALKALI-SILICA REACTION

A University Transportation Center sponsored by the U.S. Department of Transportation serving the Mountain-Plains Region. Consortium members:

Colorado State University
North Dakota State University
South Dakota State University
University of Colorado Denver
University of Denver
University of Utah
Utah State University
University of Wyoming

Technical Report Documentation Page

1. Report No.	2. Government Accession No.	3. Recipient's Catalog No.
MPC-583		

4. Title and Subtitle	5. Report Date
Composite Repair for Concrete Bridges Subjected to Alkali-Silica Reaction	March 2022
	6. Performing Organization Code
7. Author(s) Y. J. Kim	8. Performing Organization Report No. MPC 22-455
9. Performing Organization Name and Address University of Colorado Denver 1200 Larimer St Denver, CO 80217	10. Work Unit No. (TRAIS) 11. Contract or Grant No.
12. Sponsoring Agency Name and Address Mountain-Plains Consortium North Dakota State University PO Box 6050, Fargo, ND 58108	13. Type of Report and Period Covered Final Report 14. Sponsoring Agency Code

15. Supplementary Notes

Supported by a grant from the US DOT, University Transportation Centers Program

16. Abstract

This report presents a comparative experimental study on the axial behavior of concrete subjected to alkali-silica reaction (ASR) with and without confinement by carbon-fiber reinforced polymer (CFRP) sheets. A total of 120 cylinders are cast using two types of coarse aggregates to represent variable levels of ASR: rhyolite (reactive) substitutes granite (non-reactive) at a replacement ratio ranging from 0% to 100%. As per a test standard, the cylinders are conditioned in a sodium hydroxide (NaOH) solution. The physical properties of the concrete and the solution are measured over time to examine the reciprocal action between the NaOH and rhyolite, followed by microscopic observations on the progression of ASR through the concrete. Sixty cylinders are confined and all specimens are monotonically loaded to failure. The load-carrying capacity of the confined cylinders noticeably increases compared with that of the plain concrete, while the degree of improvement is controlled by the ASR-damaged concrete core. The average toughness of the cylinders decays with ASR, accompanied by irreversible energy dissipation and degraded CFRP-concrete interaction. The failure characteristics of both plain and confined cylinders are also influenced by ASR, dependent upon the replacement ratio, particularly for the integrity of the core. An analytical model is formulated to understand the implications of ASR, including an assessment of an existing design approach, and is further used for design recommendations.

17. Key Word	18. Distribution Statement
alkali silica reactions, composite materials, concrete bridges, recommendations, repairing	Public distribution

19. Security Classif. (of this report)	20. Security Classif. (of this page)	21. No. of Pages	22. Price
Unclassified	Unclassified	28	n/a

Form DOT F 1700.7 (8-72) Reproduction of completed page authorized

Composite Repair for Concrete Bridges Subjected to Alkali-Silica Reaction

Yail Jimmy Kim, Ph.D., P.Eng., FACI

University of Colorado Denver
Department of Civil Engineering

March 2022

Acknowledgments

The principal investigator gratefully acknowledges all individuals who contributed to the present research report.

Disclaimer

The contents of this report reflect the views of the authors, who are responsible for the facts and the accuracy of the information presented. This document is disseminated under the sponsorship of the Department of Transportation, University Transportation Centers Program, in the interest of information exchange. The U.S. Government assumes no liability for the contents or use thereof.

Executive Summary

This report presents a comparative experimental study on the axial behavior of concrete subjected to alkali-silica reaction (ASR) with and without confinement by carbon-fiber reinforced polymer (CFRP) sheets. A total of 120 cylinders are cast using two types of coarse aggregates to represent variable levels of ASR: rhyolite (reactive) substitutes granite (non-reactive) at a replacement ratio ranging from 0% to 100%. As per a test standard, the cylinders are conditioned in a sodium hydroxide (NaOH) solution. The physical properties of the concrete and the solution are measured over time to examine the reciprocal action between the NaOH and rhyolite, followed by microscopic observations on the progression of ASR through the concrete. Sixty cylinders are confined, and all specimens are monotonically loaded to failure. The load-carrying capacity of the confined cylinders noticeably increases compared with that of the plain concrete, while the degree of improvement is controlled by the ASR-damaged concrete core. The cylinders' average toughness decays with ASR, accompanied by irreversible energy dissipation and degraded CFRP-concrete interaction. The failure characteristics of both plain and confined cylinders are also influenced by ASR, dependent upon the replacement ratio, particularly for the integrity of the core. An analytical model is formulated to understand the implications of ASR, including an assessment of an existing design approach, and is further used for design recommendations.

TABLE OF CONTENTS

LIST OF TABLES

LIST OF FIGURES

1. INTRODUCTION

The durability of concrete structures is a salient requirement for accomplishing sustainable built-environments. Portland cement and aggregates are indispensably used to produce concrete, while their interaction frequently causes problems over time, called alkali-aggregate reaction. Once this reaction takes place, a volumetric expansion follows and the concrete cracks, leading to serviceability issues and capacity degradation. The occurrence of alkali-aggregate reactions, encompassing alkali-silica reaction (ASR) and alkali-carbonate reaction (ACR), is commonplace because aggregates account for more than 70% of a concrete mixture by volume. Unlike ACR, which is limitedly influential, ASR is considered one of the major factors that deteriorates constructed concrete (Lindgard et al. 2012). The presence of ASR typically takes five to 15 years (Spencer and Blaylock 1997), whereas ASR cracks are sometimes observed within two years of service if structures are situated in warm and humid regions (Thomas et al. 2011). Accelerated testing is generally recommended to examine the development of ASR, as specified in ASTM C1260 (ASTM 2014a) and ASTM C1778 (ASTM 2016). Although proper aggregate types and admixtures are selected, the onset of ASR is not fully addressed on many occasions. The damage resulting from ASR would not directly cause catastrophic collapse; however, structures may be demolished due to the inadequate integrity of concrete, as in the case of the Robert-Bourassa-Charest viaduct in Canada (Sanchez et al. 2012). Synergetic deterioration with other deleterious effects (e.g., freeze-thaw) may also cause undesirable performance and require considerable maintenance expenses. Besides, ASR-induced cracks accelerate the deterioration of concrete through the ingress of detrimental chemicals. A comprehensive review on the chemico-physical mechanisms of ASR and its adverse repercussions is available in state-of-the-art documents (ACI 1998; Thomas et al. 2013; Rajabipour et al. 2015).

Because the reconstruction of deficient structures is costly and time-consuming, rehabilitation is preferred in the infrastructure community (Khan 2010). Conventional methods for retarding the progression of ASR in concrete members include surface coatings, crack sealers, and lithium impregnation (Torii et al. 2004; Thomas et al. 2013). Such treatments are, however, temporary and do not restore the capacity of the damaged members. The use of carbon fiber reinforced polymer (CFRP) composites may be an alternative approach. Mohamed et al. (2006) conducted an assessment on mechanical characteristics of plain and CFRP-confined concrete cylinders mixed with reactive and non-reactive aggregates. The confinement reduced the expansion of the concrete and increased the axial capacity of the cylinders up to 314% in comparison with that of the unconfined ones. The limitation of the test campaign is that the reactive concrete was initially wrapped with CFRP and then conditioned, which may not represent the actual situation of existing concrete that had already suffered from ASR. Kubat et al. (2016) examined the performance of CFRP-confined concrete subjected to ASR. The conditioned concrete with reactive aggregates revealed a decrease in strength by 74% and elastic modulus by 93% relative to the concrete with ordinary aggregates. The application of CFRP was more effective for ASR-damaged concrete in terms of strength increase than for the undamaged concrete. These preliminary experimental investigations have shown that CFRP-confinement is a promising technique to enhance the structural behavior of ASR-activated concrete, and further signify the need for follow-up research, particularly concerning the interaction between ASR and CFRP-confined concrete as well as the development of design provisions.

This study discusses a test program aiming to elucidate the migration of ASR in concrete, the relationship between the progression of ASR and the response of CFRP-confined concrete, and failure specifics. Performance-based efficiency factors are proposed to translate research into practice.

2. RESEARCH SIGNIFICANCE

The performance of CFRP-confined concrete that has been exposed to an aggressive service environment (prior to strengthening) is reliant upon the quality of the core. When concrete is impaired by ASR, the structure of the constituents becomes unstable, followed by a volumetric expansion and micro-cracking in the cement paste. Accordingly, the knowledge of CFRP-confinement established with ordinary concrete may not be sufficient for ASR-affected concrete; moreover, published design guidelines do not render any information (*fib* 2001; ACI 2017; CSA 2017). The present research intends to understand the effects of ASR on the behavior of concrete confined with CFRP and suggests a methodology for practitioners to implement.

3. TEST PROGRAM

3.1 Materials

General purpose portland cement (Type I, ASTM 2018) was the binder of concrete. Two types of aggregates were used to examine the implications of ASR: granite and rhyolite (Figure 3.1[a]). The ordinary aggregate, granite, is readily available for a construction project and is not alkali-silica reactive (Ng and Beng 2007). In accordance with the supplier's data sheet, granite has a compressive strength of 200 MPa (29,000 psi), a density of 2,700 kg/m^3 (4,550 lb/yd^3), and an average hardness of 6.5 on the Mohs hardness scale. Rhyolite is a reactive material (Sirivivatnanon et al. 2016), consisting of quartz, plagioclase, and sanidine, and has the following supplier-provided properties: compressive strength = 140 MPa (20,300 psi), density = 2,500 kg/m^3 (4,210 lb/yd^3), and hardness = 6.5. Fine aggregate was natural sand with a maximum size of 4.75 mm (0.187 in.), No. 4 sieve. CFRP sheets comprising unidirectional carbon fiber fabrics and an epoxy matrix were produced by a wet lay-up process (dry fabrics are impregnated in the epoxy and cured to form a composite). The sheets have a guaranteed tensile strength of 3,800 MPa (550 ksi) with a modulus of 227 GPa (33,000 ksi) at a rupture strain of 0.0167, based on an equivalent fiber thickness of 0.165 mm (0.006 in.). The matrix was mixed with a hardener and a resin at a volume ratio of 1:3 and stirred until a homogenous mixture was obtained. After seven days of curing, the hardened epoxy has a nominal tensile strength of 52 MPa (7,540 psi), an elastic modulus of 2.6 GPa (380 ksi), and an elongation of 0.015 at break.

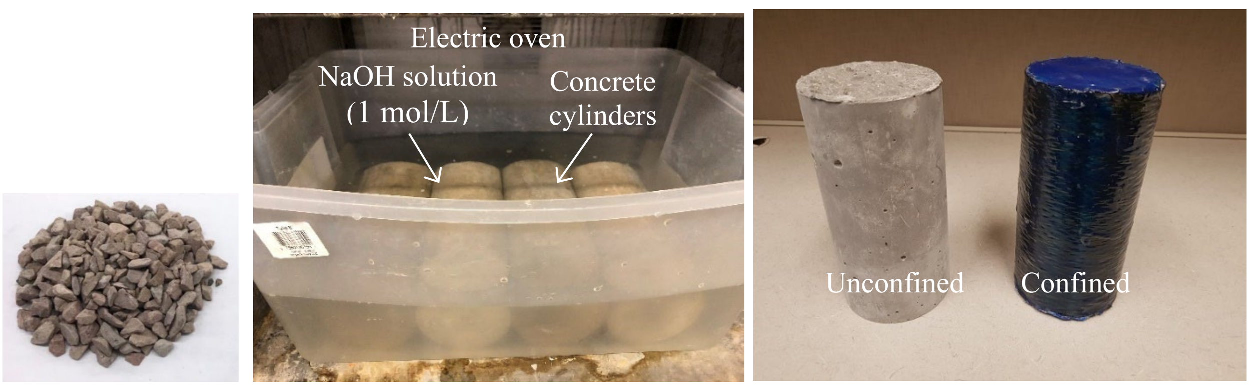

(a) (b) (c)

[1 mol/L = 3.6 mol/gallon; $^oF = (^oC \times 9/5) + 32$]

Figure 3.1 Specimens and conditioning: (a) coarse aggregates; (b) immersion in NaOH solution; (c) concrete cylinders with and without CFRP-confinement

3.2 Conditioning and Specimens

3.2.1 ASR-Activation

A sodium hydroxide (NaOH) solution was prepared at a concentration of 1 mol/L (3.6 mol/gallon); a 40-gram (0.09-lb) NaOH solid was dissolved in a beaker containing 900 ml (0.24 gallons) of distilled water and gradually adjusted to 1,000 ml (0.26 gallon). To activate ASR reactions, as specified by ASTM C1260 (ASTM 2014a), test specimens were submerged in the solution at 80^{o}C (176^{o}F) for up to 28 days (an electric oven was utilized). ASTM C1778 (ASTM 2016) acknowledges that ASTM C1293 (ASTM 2008) may not be practical for ASR examinations due to the long conditioning duration.

3.2.2 Concrete

A total of 120 cylinders (100 mm [4 in.] in diameter by 200 mm [8 in.] in depth) were cast as per the mixture designs detailed in Table 3.1. To control variable degrees of ASR, the ordinary granite aggregate was substituted by rhyolite at a replacement ratio of 0% to 100%. Upon curing in a humidity room for 28 days (50% relative humidity at 23°C [73°F]), the cylinders were dried and airbrushed to eliminate unnecessary substances. Three exposure categories were then tested pursuant to ASTM C1260 (ASTM 2014a), except for the control specimens (0 days), all cylinders were conditioned for 14 and 28 days (Figure 3.1[b]) as delineated above (NaOH at 80°C [176°F]). After completing those exposure periods, the cylinders cooled to room temperature and were cleaned; thereafter, they were classified into plain and confined groups (60 cylinders each). For the cylinders appertaining to the confined group, the premixed epoxy adhesive was uniformly applied to the concrete surface using a spatula and a single layer of carbon fabric sheet (200 mm [8 in.] wide by 340 mm [13 in.] long) was impregnated at an overwrapping length of 25 mm (1 in.) in the circumferential direction, as shown in Figure 3.1(c). The entrapped air and epoxy residues in the CFRP composite were squeezed out with a hand roller. To preclude potential chemical reactions between the conditioned concrete and ambient air during the CFRP curing (seven days at room temperature), the top and bottom surfaces of the CFRP-confined cylinders were covered by the epoxy.

Table 3.1 Details of concrete mixture ratio [1 kg/m^3 = 1.69 lb/yd^3]

Category (replacement ratio)	Cement (kg/m^3)	Water (kg/m^3)	Rhyolite (kg/m^3)	Granite (kg/m^3)	Fine aggregate (kg/m^3)
0% (0% rhyolite +100% granite)	1	0.45	0	2.88	1.26
25% (25% rhyolite + 75% granite)	1	0.45	0.72	2.16	1.26
50% (50% rhyolite + 50% granite)	1	0.45	1.44	1.44	1.26
75% (75% rhyolite +25% granite)	1	0.45	2.16	0.72	1.26
100% (100% rhyolite + 0% granite)	1	0.45	2.88	0	1.26

3.3 Test Methods and Instrumentation

3.3.1 Sieve Analysis

Complying with ASTM C136 (ASTM 2014b), sieve analysis was conducted to grade the granite and rhyolite aggregates. Considering the size of the concrete cylinders, aggregates greater than 27 mm (1.06 in.) were removed prior to casting.

3.3.2 Digital Image Processing

A state-of-the-art imaging technique was utilized to determine the size distribution of the coarse aggregates. A piece of black paper was placed on a laboratory table to reduce the reflection of light, as shown in Figure 3.2(a), and the respective aggregates were randomly spread. The illumination lamps positioned 180 degrees apart improved the quality of digital imaging underneath the aggregates without shadows. A high-resolution camera with 24 million pixels took pictures and the images were converted to a binary format (Figure 3.2[b]). A Java-based platform, *ImageJ* (Ferreira and Rashband 2012), processed the image files, quantified particle sizes, and generated histograms.

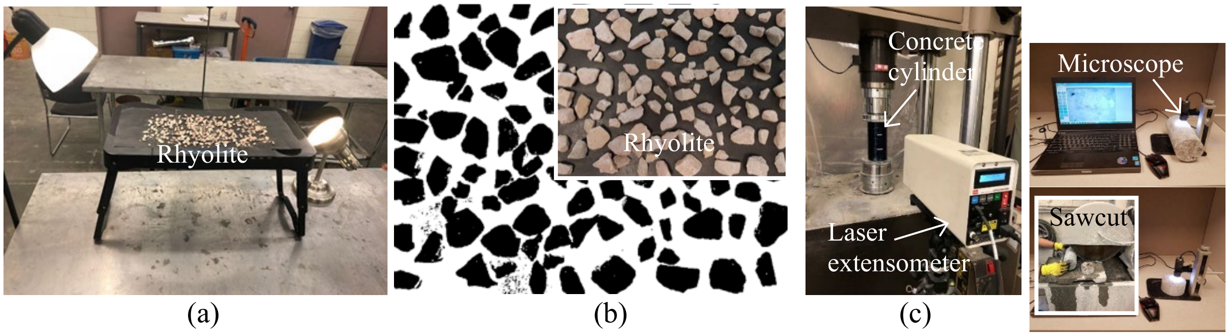

(a) (b) (c)

Figure 3.2 Test methods: (a) image sampling for rhyolite; (b) raw and binary images; (c) cylinder compression; (d) microscopy on concrete cylinder and disk

3.3.3 Mass and pH

The mass of each concrete cylinder was monitored at a seven-day interval, except for the very first day of ASR-activation. Before measuring the mass, the liquid on the cylinder surface was wiped off with paper towels. To minimize the disruption of the planned conditioning schedule, the cylinders were immediately restored to the container in the electric oven heated at 80ºC (176ºF). The potential of hydrogen (pH) in the solution was also regularly measured every seven days (five times per measurement) using a digital pH meter at an accuracy of ±0.02 pH.

3.3.4 Concrete Cylinder Test

The conditioned cylinders were monotonically loaded at a rate of 5 mm/min (0.2 in./min) to study the effects of ASR on the compressive strength and the efficacy of CFRP-confinement (Figure 3.2[c]). For strain measurement employing a non-contacting laser extensometer with a resolution of 0.001 mm (0.00004 in.), reflection tapes were attached to the middle-third points of the individual cylinders.

3.3.5 Digital Microscopy

Deterioration of the concrete was evaluated on the surface level by a digital microscope (at 0, 14, and 28 days of exposure, Figure 3.2[d]). The microscope is equipped with a CMOS sensor and generates 1,280-by-1,024-pixel images at 30 frames per second. After trial scanning, a 100 times magnification was selected. To investigate the penetration of the NaOH solution through the concrete (formation of ASR gels, contingent upon exposure period), selected cylinders were cut to a depth of 50 mm (2 in.) with a diamond saw (Figure 3.2[d], inset); then, the cross-sectional surface was pictured (Figure 3.2[d]).

4. EXPERIMENTAL RESULTS

4.1 Aggregate Distribution

Figures 4.1(a) and (b) compare the size of the granite and rhyolite aggregates, respectively. It is known that the compressive strength of concrete depends upon the size of coarse aggregate (Meddah et al. 2010). The distributions obtained from the image and sieve analyses were analogous at an average difference of 17% and 9% for the granite and rhyolite, respectively, both of which showed a maximum particle size of 16 mm (0.63 in.). The comparison between these aggregates exhibited a difference of 14%, on average (Figure 4.1[c]), including a difference of 4% at the size of 16 mm (0.63 in.). This fact ensures that the implications incurred by aggregate size would be marginal on the strength development of the ASR-activated cylinders.

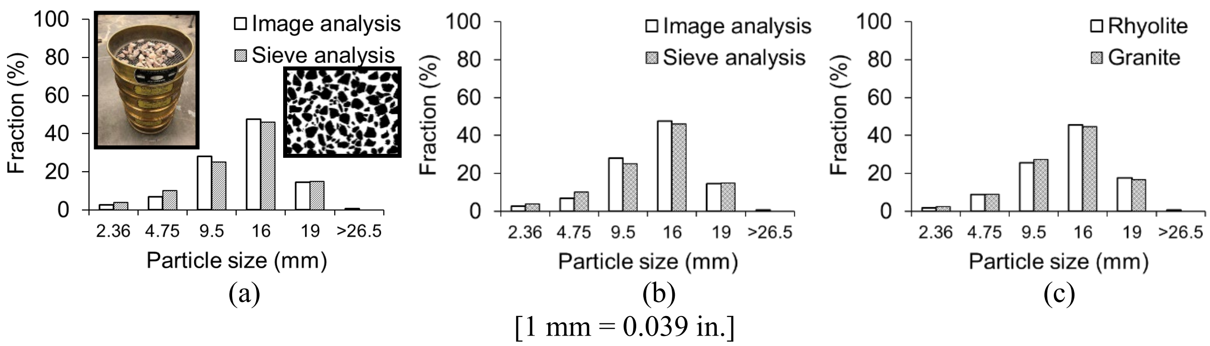

Figure 4.1 Particle size distribution: (a) granite; (b) rhyolite; (c) comparison based on image analysis

4.2 Concrete Response

4.2.1 Physical Properties

The variation of concrete mass with variable aggregate-replacement ratios is detailed in Figure 4.2(a). Regardless of the replacement ratio, the mass increased from 0 days to 1 day because of capillary action that absorbed the NaOH solution (Lindgard et al. 2012). Afterward, the increment pattern was affected by the amount of rhyolite. The cylinders with a replacement ratio of 100% exhibited a consistent increase in mass from 1 day to 28 days. Such an ascending propensity was valid up to 21 days for those with a replacement ratio of 75%, below which the mass variation was insusceptible to the replacement ratio (that is, plateau-like responses were recorded from 0% to 50%). Figure 4.2(b) compares the time-dependent mass of the individual categories normalized by the control mass at 0 days. The difference among those specimens became noticeable after 7 days, especially for the cylinders with 75% and 100% replacement ratios. It is thus stated that the liquid-solid interaction between the NaOH and concrete had a threshold replacement ratio of 50% (the replacement ratio is equated with the extent of ASR-development). The chemical responses of the solution with time are plotted in Figure 4.2(c) where a gradual decrease in the potential of hydrogen (pH) was logged. The magnitude of the reduction was a function of the rhyolite replacement ratio (Figure 4.2[d]). Chemical analysis clarifies that a change in siloxane bond due to hydroxyl (Glasser 1992) and the ionized $Si(OH)_4$ (Sjoberg 1996) are responsible for lowering the pH values. The decreased pH is another indicator of the increased ASR in tandem with ion exchanges (Rajabipour et al. 2015).

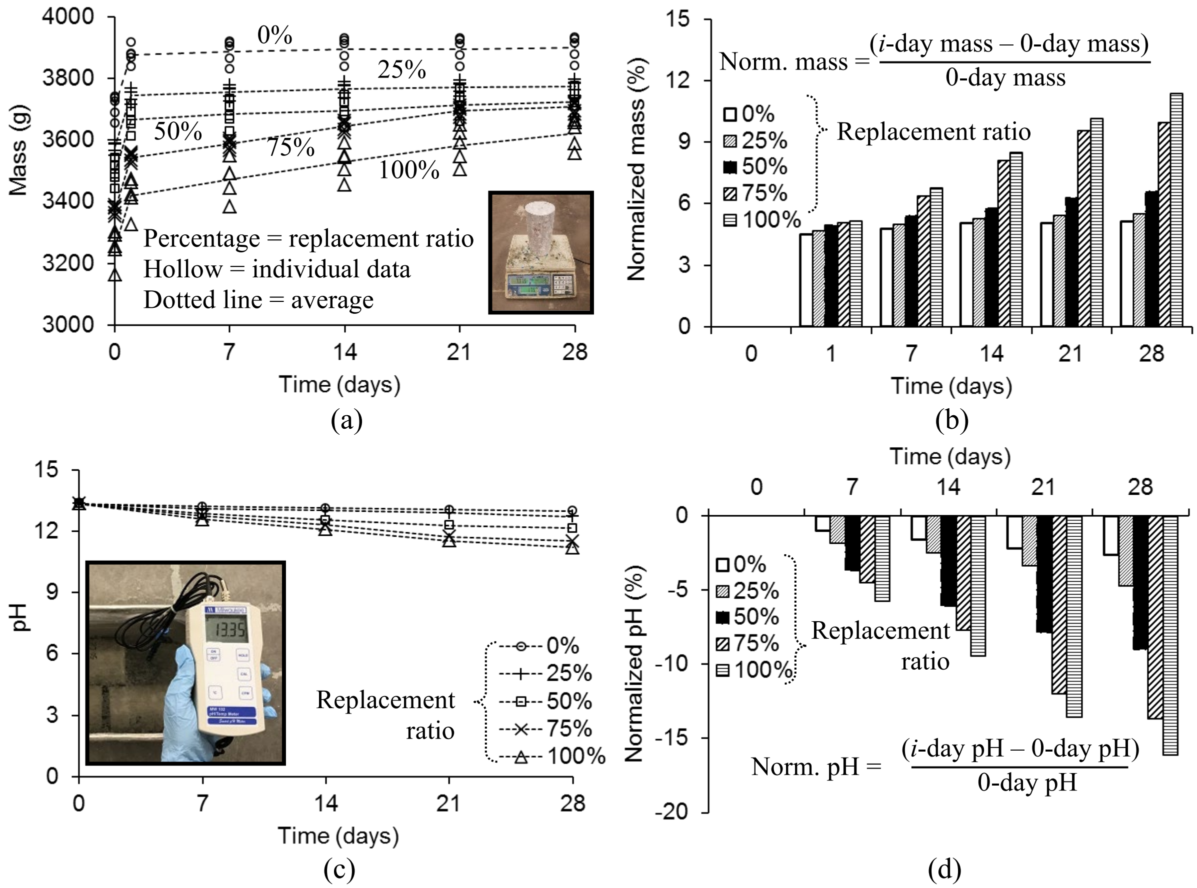

[1 g = 2.2 lb]

Figure 4.2 Time-dependent physical properties: (a) concrete mass; (b) change of mass; (c) potential of hydrogen (pH); (d) change of pH

4.2.2 Surface-Level Deterioration

Pictured in Figure 4.3 is the surface of the concrete cylinders exposed to the NaOH solution. Notwithstanding the slight decoloring at 28 days of conditioning, the texture of the control specimen with a 0% replacement showed insignificant changes (Figure 4.3[a]). As the replacement ratio was increased to 50% (Figure 4.3[b]), the concrete surface at 14 and 28 days altered with the dissolved cement paste, which implies that the chemical reaction between the near-surface rhyolite aggregates and the solution had begun. The texture pattern of the concrete with a 100% replacement at 14 days (Figure 4.3[c]) was comparable to the pattern of the 50% replacement concrete at 28 days (Figure 4.3[b]), whereas a distinct morphology was noticed at 28 days (Figure 4.3[c]). These microscopic assessments mean that the ASR products, which were generated by the diffused hydroxyl ions interacting with the reactive aggregates (Dyer 2014), migrated through the cement paste and transformed the geometric appearance of the concrete (supplementary discussions are provided in the subsequent section).

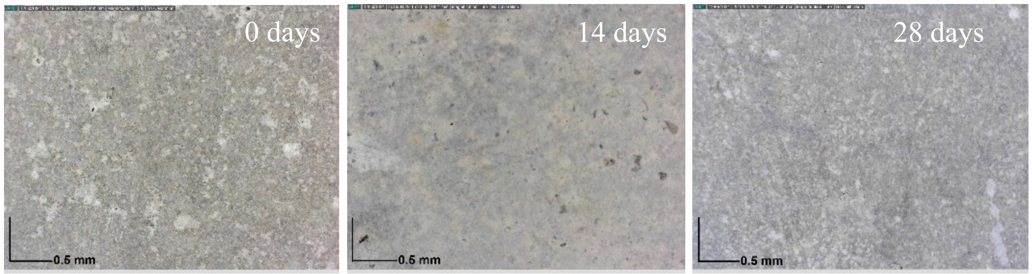

(a)

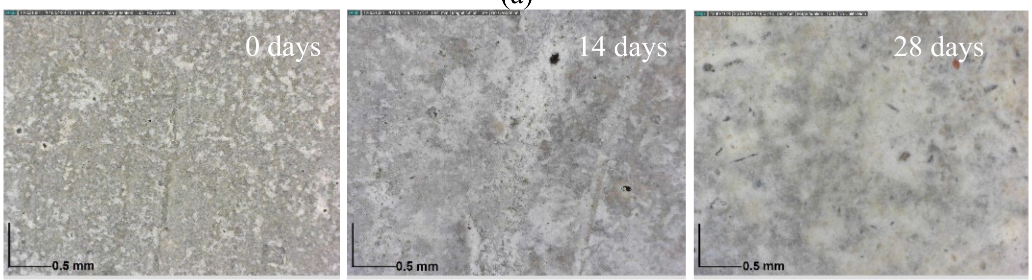

(b)

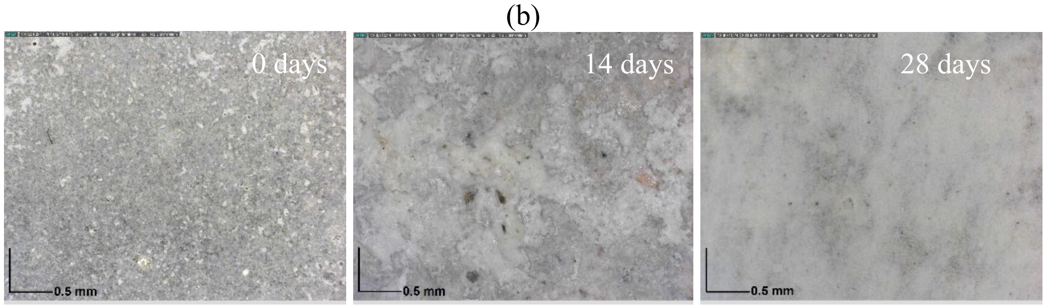

(c)

[1 mm = 0.039 in.]

Figure 4.3 Microscopic images of concrete surface subjected to NaOH (100 times magnification): (a) 0% replacement; (b) 50% replacement; (c) 100% replacement

4.2.3 Formation of ASR-Gel

The images taken from the concrete disks (13 mm [0.5 in.] from the surface) are given in Figure 6. Despite the NaOH exposure, detrimental changes were not noticed in the control mixture without rhyolite (Figure 4.4([a]). The micrographs of the concrete with a 50% replacement ratio until 14 days were akin to those of the 0% specimens; however, a hygroscopic ASR gel in the micro-cracked cement paste was detected at 28 days, as shown in Figure 4.4(b). These time-dependent transitions are attributable to alkaline hydroxides in the pore solution (Neville 1995). For the specimens with a 100% replacement ratio (Figure 4.4[c]), the reactivity between the alkalis and silica was substantial; accordingly, the formation of ASR gels was conspicuous. The width of the ASR gels was about 0.1 mm (0.0039 in.), similar to the values reported by others (Giaccio et al. 2008). This observation indicates that the diffused solution through the hydrated cement paste, alongside the permeation of the NaOH solution, accelerated the chemical reactions and led to the swelling of the concrete. Even if no visible cracks were noticed, the microstructure of the cement matrix became unstable owing to the presence of the ASR gels, accompanied by a silica dissolution process (Mehta and Monteiro 2014).

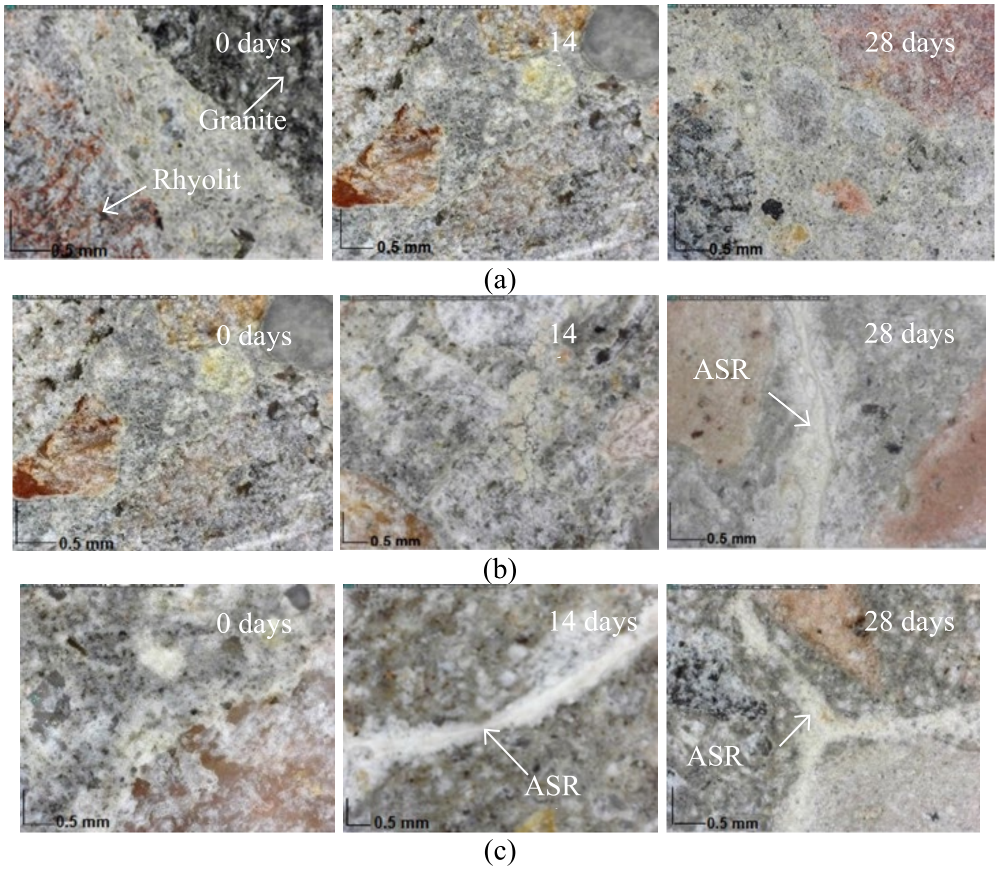

[1 mm = 0.039 in.]

Figure 4.4 Microscopic images of concrete cross section subjected to NaOH (100 times magnification): (a) 0% replacement; (b) 50% replacement; (c) 100% replacement

4.3 Axial Behavior of Concrete

4.3.1 Constitutive Relationship

The axial stress of the plain cylinders increased with strain in a linear manner, as shown in Figure 4.5(a). Since the behavior of the specimens was analogous in all exposure periods, only those exposed to 28 days were provided for brevity. The response fluctuations were ascribed to the local instability of the concrete within the monitored region; micro-cracks occurred owing to the local stresses inside the concrete, which were randomly transferred to the cement binder between aggregates, and thus the positions of the reflection tapes for the non-contacting laser extensometer were affected. Regarding the confined cylinders (Figure 4.5[b]), the stresses precipitously developed up to about 60 MPa (8,700 psi) at which a bilinear transition took place. The slope of the case with a 100% replacement ratio was lower than those of the others. Given that CFRP-confinement is activated after the core sufficiently damages and dilates (ACI 2017), the 100%-replacement specimen appears to undergo extensive ASR-induced damage.

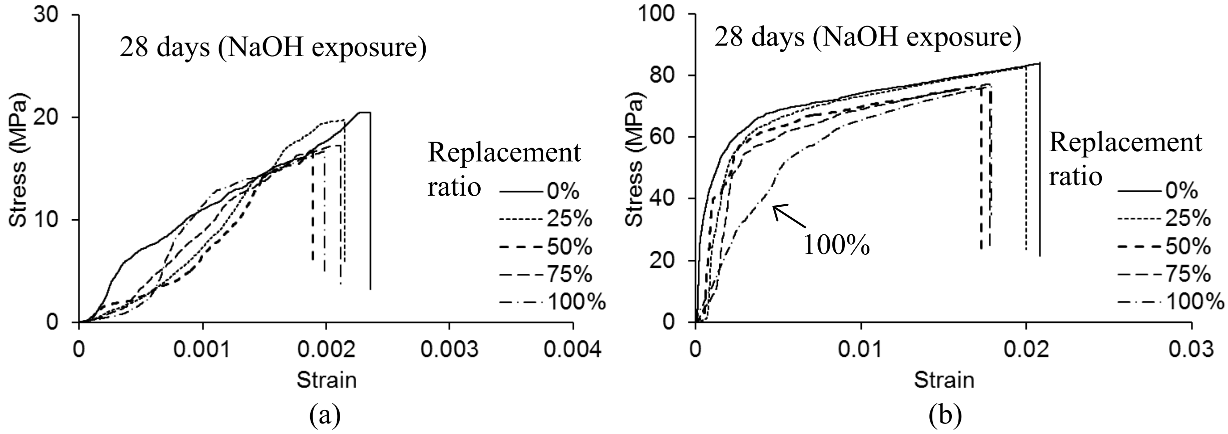

[1 MPa = 145 psi]

Figure 4.5 Stress-strain behavior of cylinders: (a) plain concrete; (b) CFRP-confined concrete

4.3.2 Load-Carrying Capacity

Figure 4.6(a) compares the stress of the plain concrete cylinders at failure, dependent upon replacement ratio and exposure period. The cylinders without reacting to NaOH (0 days) maintained the axial capacity, irrespective of rhyolite amount, which denotes that the strength of the concrete mixed with the rhyolite and granite aggregates was not different. As the exposure period increased, the load-carrying capacity of the cylinders dwindled due to the activation of ASR. For clarity, the average capacities of the individual categories are shown in Figure 4.6(b). Regarding the confined cylinders (Figure 4.6[c]), the capacities elevated in all cases relative to those of the plain concrete cylinders. The strength reduction with exposure time (Figure 4.6[d]) signifies the deleterious consequences of ASR in the confined cores. Figure 9 further explicates the influence of the replacement ratio, equivalent to the degree of ASR damage. To facilitate assessments, the axial strength of the cylinders was normalized by that of the control cylinder (0% replacement) without experiencing ASR (0 days). For the unstrengthened concrete under 14-day exposure (Figure 4.7[a]), the strength drop was less than 5% up to a replacement ratio of 50%, beyond which a large reduction was noticed. As the exposure period was increased to 28 days, the reduction pattern became linear, implying that the interaction between the rhyolite and NaOH solution was significant even at a replacement ratio of 25%. The normalized strength of the confined concrete subjected to 14-day exposure was maintained below 5% up to a replacement ratio of 75% (Figure 4.7[b]). The 28-day-exposure concrete confined with CFRP also revealed a linear response with the replacement ratio; however, the strength reduction was not as prominent as its plain counterpart. The effectiveness of CFRP-confinement was, therefore, substantiated by the capacity preservation of the ASR-activated concrete core.

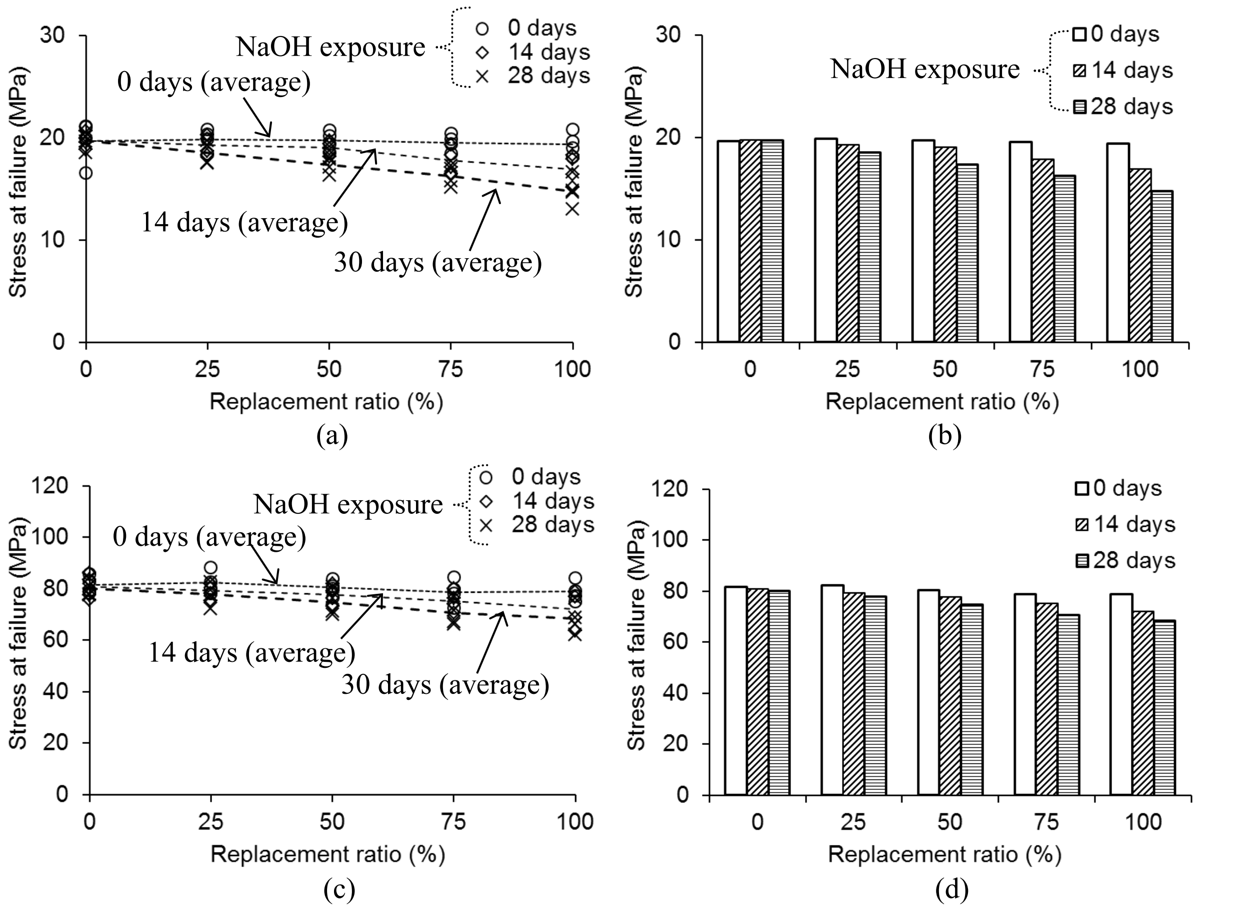

[1 MPa = 145 psi]

Figure 4.6 Capacity of concrete: (a) failure stress of plain concrete; (d) average load-carrying capacity of plain concrete; (c) failure stress of CFRP-confined concrete; (d) average load-carrying capacity of CFRP-confined concrete

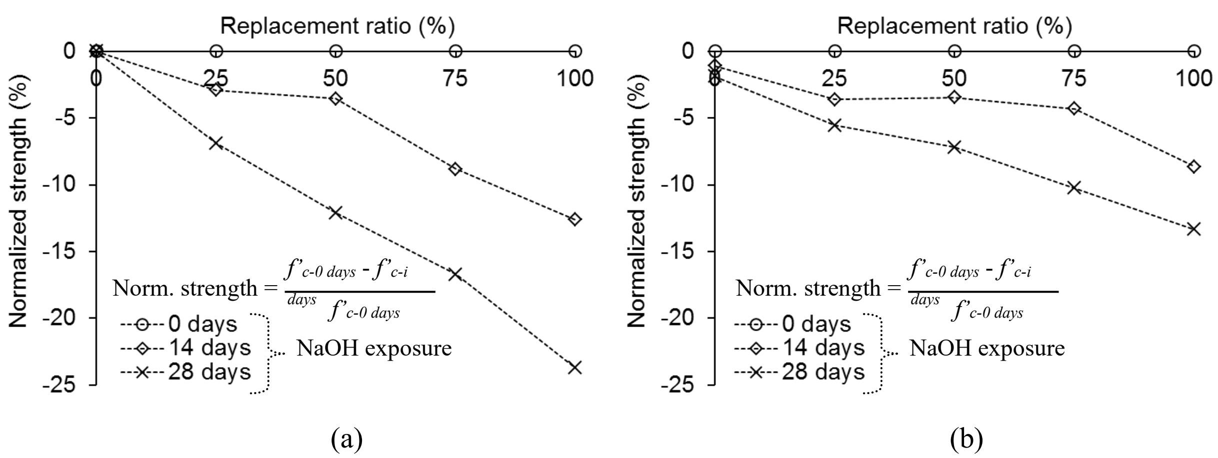

Figure 4.7 Effects of ASR-induced damage (f'_c = average strength): (a) unconfined concrete; (b) confined concrete

4.3.3 Toughness

The toughness of each cylinder was obtained by integrating the area under the individual stress-strain curve up to the peak stress and is summarized in Figure 4.8. For the plain cylinders (Figure 4.8[a]), scatter was observed owing to the random reaction of rhyolite with NaOH (that is, non-deterministic activation of ASR). The variation of the average toughness at 0 days and 14 days was virtually independent of the replacement ratio; however, the average toughness at 28 days was reduced with the ratio (Figure 4.8[b]). Considering that toughness is equated to the strain energy of a system from a mechanics perspective, such a decreasing trend in the 28-day specimens indicates the occurrence of irreversible energy dissipation during the chemical process of ASR. Upon CFRP-confining, the toughness of the concrete markedly increased (Figure 4.8[c]). Similar to the plain concrete specimens, the average toughness values at 0 days were almost invariant; by contrast, those of the 14- and 28-day specimens steadily decayed with the increased amount of rhyolite (Figure 4.8[d]). This is explained by the inherent damage of the core concrete: since the CFRP system was activated after reaching the ultimate strength of the core concrete, as elaborated above, the load-bearing mechanism of the confined cylinder was reliant upon the reciprocal action between the degraded core and CFRP. In other words, the level of the CFRP-core interaction diminished as the ASR damage augmented.

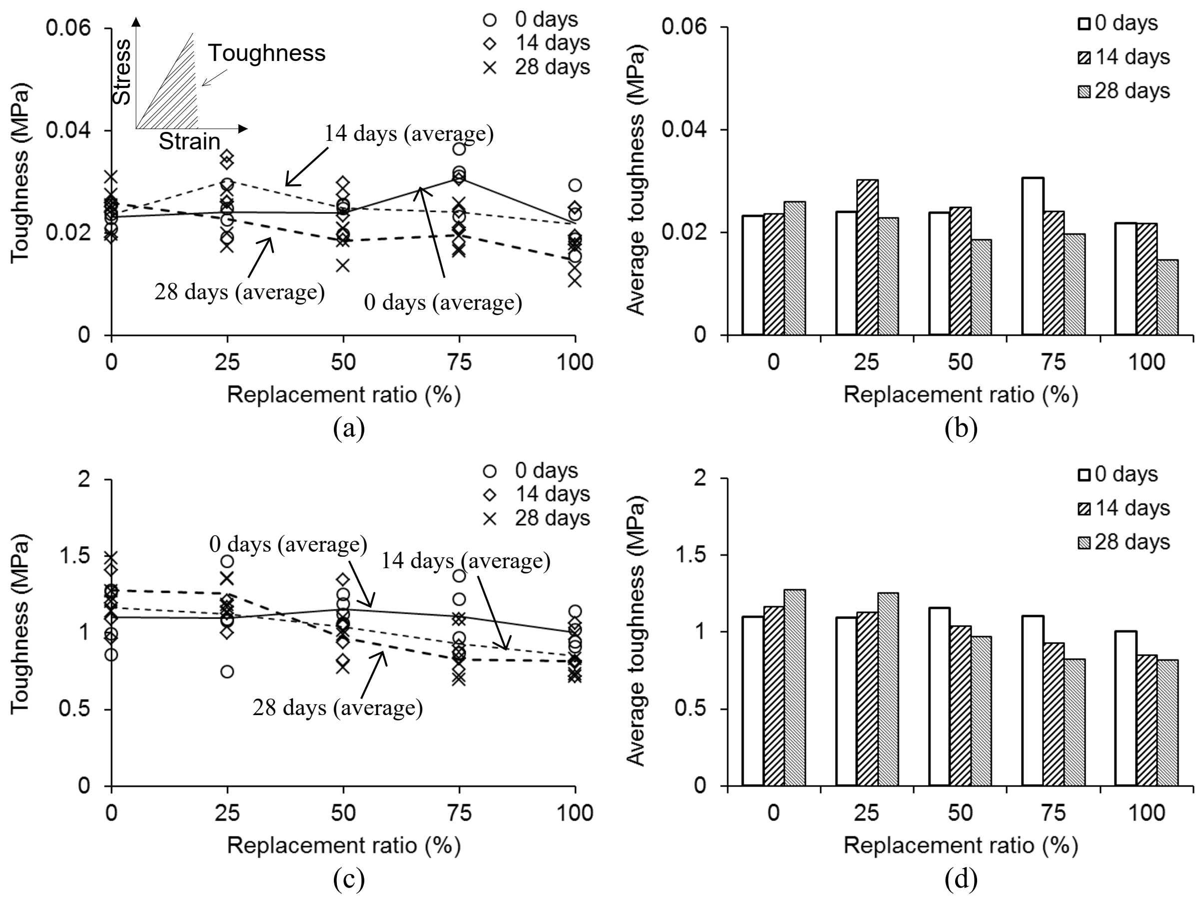

[1 MPa = 145 psi]

Figure 4.8 Comparison of toughness: (a) plain concrete; (b) average of plain concrete; (c) CFRP-confined concrete; (d) average of CFRP-confined concrete

4.4 Failure Mode

4.4.1 Plain Concrete

Figure 4.9 shows the failure mode of the plain cylinders with a focus on the aggregate replacement ratio and exposure period. At a 0% replacement ratio without rhyolite, the cylinders failed by a localized crack that grew in the vertical direction (Figure 4.9[a]). When the NaOH-exposure time increased, the concrete disintegrated (28 days in Figure 4.9[a]). The effects of ASR-activation became pronounced in the cylinders with 25% and 50% replacement ratios at 14 and 28 days (Figures 4.9[b] and [c]) along with large concrete spalling. The 0-day-exposure specimens with replacement ratios of 75% and 100% revealed multiple cracks (Figures 4.9[d] and [e]), which were not noticed in the 0-day specimens with lower replacement ratios, possibly because of the difference in bond performance between the rhyolite and granite with the cement binder (specifically, their distinct behavior in the interfacial transition zone). Further research may clarify this hypothesis although there is no accepted test method to evaluate the bond of aggregates (Neville 1995). The failure of the ASR-activated concrete with the 75% and 100% ratios involved considerable disintegration, explaining the reason why the strength of these cylinders was substantially lower in Figure 4.6(a) and (b).

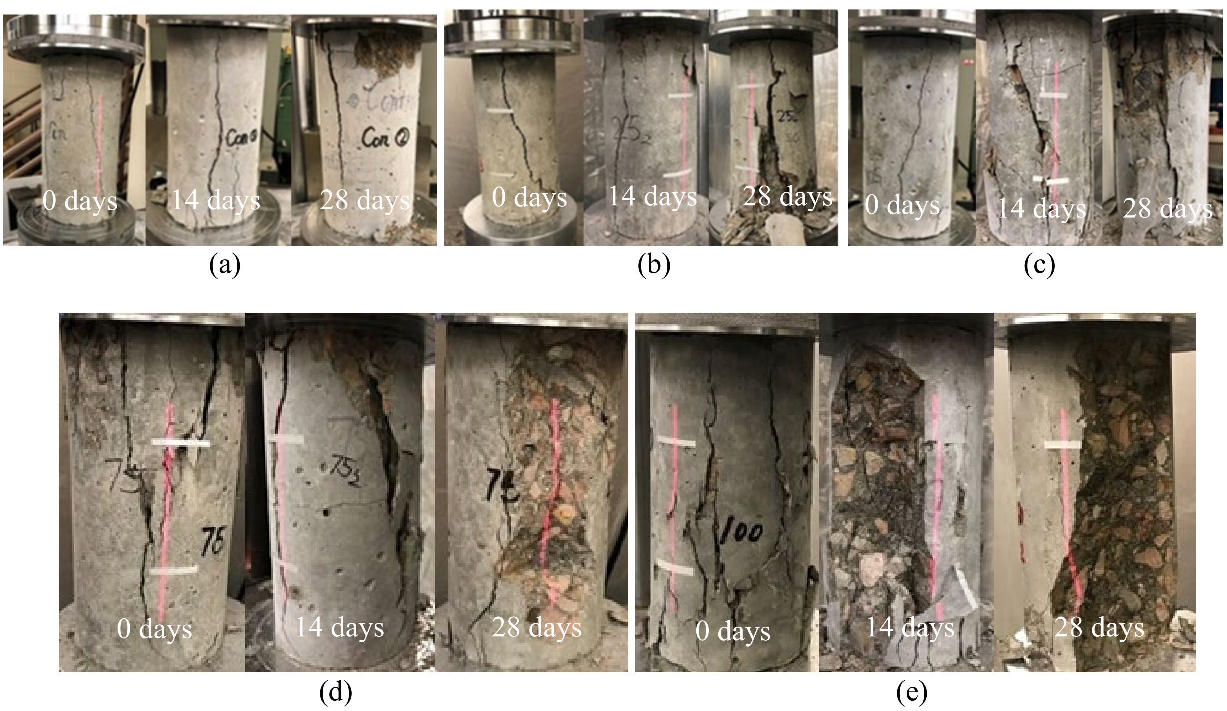

Figure 4.9 Failure modes of plain concrete subjected to NaOH: (a) 0% replacement; (b) 25% replacement; (c) 50% replacement; (d) 75% replacement; (e) 100% replacement

4.4.2. CFRP-Confined Concrete

The failure of the confined concrete is available in Figure 4.10. The cylinders with replacement ratios of 0% to 50% exhibited modest CFRP-rupture at 0 days, while those at 14 and 28 days showed much larger rupture zones (Figures 10[a] to [c]). The amount of concrete-spalling from the cylinders at 28 days was independent of the replacement ratio up to 50%, which was drastically different from the spalling tendency of the plain cylinders (Figures 4.9[a] to [c]); hence, the CFRP-confinement was proven to be effective in preserving the integrity of the ASR-damaged concrete core within the 0% to 50% replacement range. On the contrary, as the amount of rhyolite was increased over 75%, the failure of the confined cylinders was explosive, and the core concrete crumbled (Figures 4.10[d] and [e]). This observation illustrates that the internally stored energy abruptly dissipated when the CFRP ruptured, thereby shattering the core concrete.

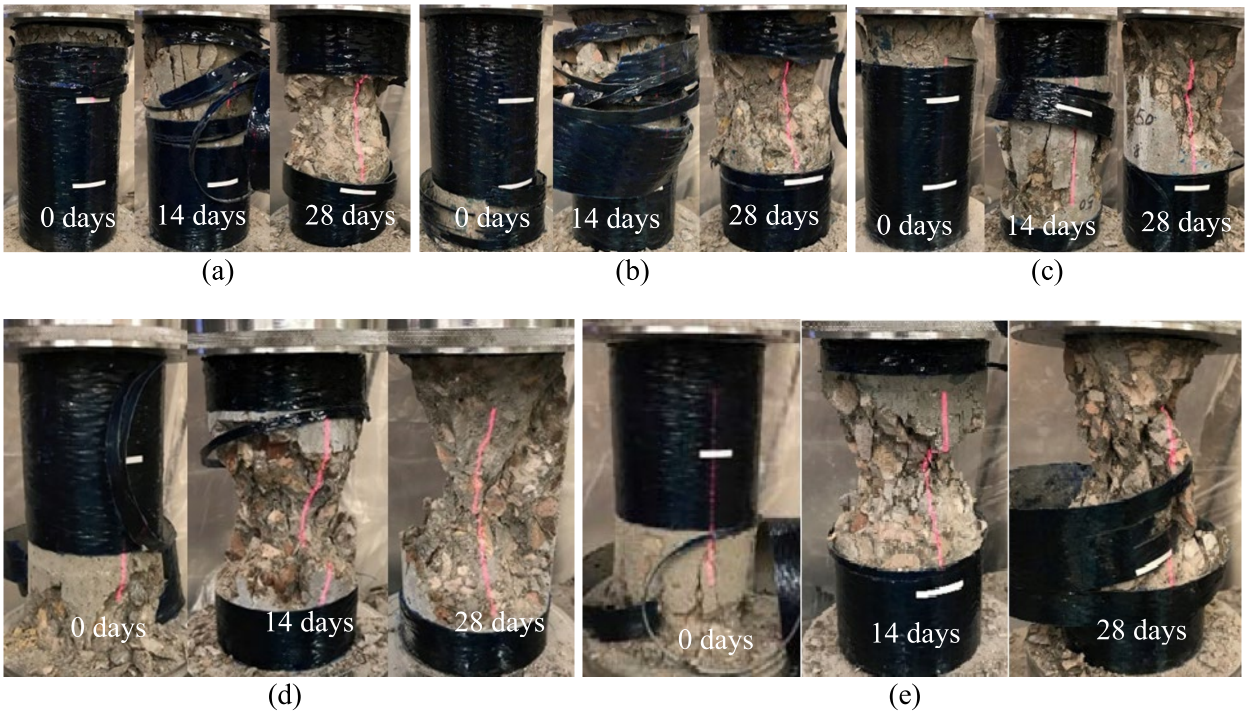

Figure 4.10 Failure modes of CFRP-confined concrete subjected to NaOH: (a) 0% replacement; (b) 25% replacement; (c) 50% replacement; (d) 75% replacement; (e) 100% replacement

5. MODELING AND DESIGN RECOMMENDATIONS

5.1 Model Development

The strength of concrete subjected to ASR damage may be expressed by (Saouma and Perotti 2006)

$$f_c(t,T) = f_{c0}\left[1 - (1-\beta_f)\xi(t,T)\right] \tag{1}$$

$$\beta_f = f_c(t,T) / f_c(0,T) \tag{2}$$

where $f_c(t,T)$ is the degraded compressive strength at time t and temperature T; f_{c0} is the initial strength without ASR; β_f is the residual strength factor; and $\xi(t,T)$ is the chemical reaction factor, which may be determined by (Ulm et al. 2000)

$$\xi(t,T) = \frac{1-\exp(-t/\tau_c(T))}{1+\exp(-t/\tau_c(T)+\tau_L(T)/\tau_c(T))} \tag{3}$$

$$\tau_c(T) = \tau_c(T_0)\exp\left[U_c(1/T - 1/T_0)\right] \tag{4}$$

$$\tau_L(T) = \tau_L(T_0)\exp\left[U_L(1/T - 1/T_0)\right] \tag{5}$$

where $\tau_c(T)$ and $\tau_L(T)$ are the characteristic and latency time factors at temperature T in Kelvin, respectively; and U_c and U_L are the activation energies related to the time factors (U_c = 5,400K and U_L = 9,400K, Ulm et al. 2000). The reference temperature was set to room temperature (T_0 = 293K), which resulted in the characteristic and latency time factors of $\tau_c(T_0)$ = 55 days and $\tau_L(T_0)$ = 357 days based on (Ulm et al. 2000)

$$\tau_c(T_0) = 6\times10^{-7}\exp(5373.3/T_0) \tag{6}$$

$$\tau_L(T_0) = 4\times10^{-12}\exp(9411.9/T_0) \tag{7}$$

The strength of the confined concrete, f_{cc}, can be generalized by (for convenience, the time and temperature terms (t, T) are not marked hereafter)

$$\frac{f_{cc}}{f_c} = 1 + k_1\left(\frac{f_l}{f_c}\right)^{k_2} \tag{8}$$

$$f_l = \frac{2E_f n t_f \kappa_\varepsilon \varepsilon_{fu}}{D} \tag{9}$$

where k_1 and k_2 are empirical constants, f_l is the confining pressure; E_f, t_f, and ε_{fu} are the elastic modulus, single-ply thickness, and rupture strain of the CFRP, respectively; n is the number of CFRP layers; κ_ε is the CFRP efficiency factor (κ_ε = 0.55, ACI 2017); and D is the diameter of the cylinder. ACI 440.2R-17 (ACI 2017) provides the following equation to predict the strength of the confined concrete

$$\frac{f_{cc}}{f_c} = 1 + \psi_f 3.3\kappa_a \left(\frac{f_l}{f_c}\right) \tag{10}$$

where ψ_f and κ_a are the reduction and geometry factors, respectively (ψ_f = 0.95 and κ_a = 1.0, ACI 2017). Adding an adjustment factor (ψ_{adj}) to address the use of the empirical constants involved in Eq. 10 and comparing the CFRP-related terms between Eqs. 8 and 10 yield

$$k_1 \left(\frac{f_l}{f_c}\right)^{k_2} = \psi_{adj} \psi_f 3.3\kappa_a \left(\frac{f_l}{f_c}\right) \tag{11}$$

An adjustment factor, which accounts for the ASR effects in using the empirically calibrated ACI 440.2R-17 equation, is obtained

$$\psi_{adj} = \frac{k_1 \left(\frac{f_l}{f_c}\right)^{k_2}}{\psi_f 3.3\kappa_a \left(\frac{f_l}{f_c}\right)} \tag{12}$$

5.2 Implementation

To attain the residual strength factor β_f in Eq. 2, a regression analysis was conducted using the test data at T = 80ºC (176ºF) as specified earlier

$$f_c(t) \text{ or } f_{cc}(t) = A\exp(B \times t) \tag{13}$$

where A and B are regression constants (calibrated constants are listed in Table 5.1). Figure 5.1(a) shows the variation of the concrete strength, contingent upon the implications of ASR (that is, the replacement ratio). After calibrating the regression constants for the confined concrete (Table 5.1), the strength ratio of f_{cc}/f_c is plotted in Figure 13(b). It is apparent that the efficacy of CFRP-strengthening went up as ASR progressed, which should be taken into consideration when confining deteriorated concrete members. Figure 5.1(c) exhibits the empirical constants k_1 and k_2 calibrated by an optimization technique (general reduced gradient is a method; details are available elsewhere, Lasdon et al. 1973) in conjunction with Eqs. 8 and 9 alongside Eq. 13. The degree of variation in these constants was marginal; consequently, their averaged values may be used for practice: k_1 = 4.72 and k_2 = 0.40. The adjustment factor for ASR is then acquired and graphed in Figure 13(d). The decreasing trend of the ψ_{adj} factor over time (representing the development of ASR) illustrates the augmented discrepancy between the strength predicted by the ACI 440.2R-17 equation and the confined strength of the ASR-damaged concrete.

Table 5.1 Regression constants

Replacement ratio (%)	A		B	
	Unconfined	Confined	Unconfined	Confined
0	20.058	81.593	-7×10^{-4}	-7×10^{-4}
25	19.903	81.298	-3×10^{-3}	-2×10^{-3}
50	19.904	80.484	-5×10^{-3}	-3×10^{-3}
75	19.531	79.401	-7×10^{-3}	-4×10^{-3}
100	19.378	78.750	-1×10^{-2}	-5×10^{-3}

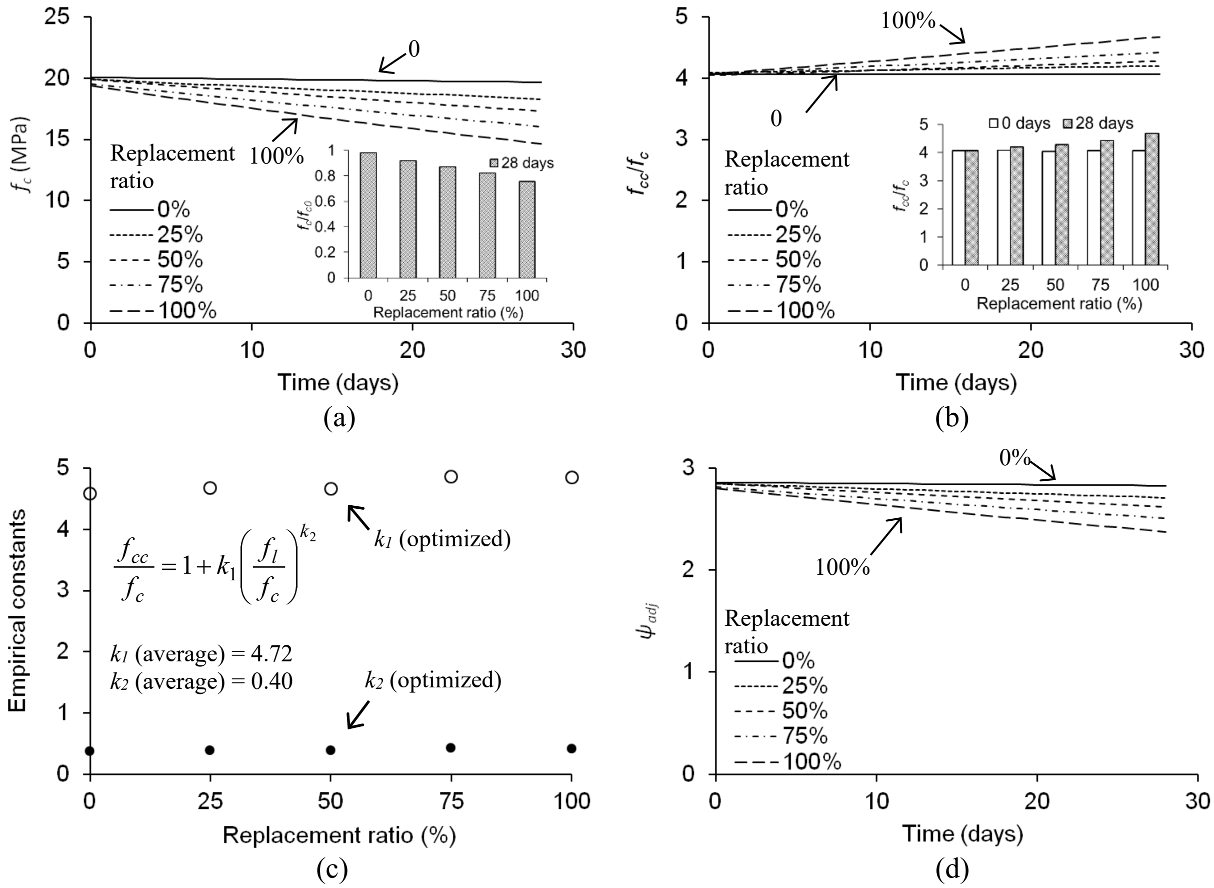

[1 MPa = 145 psi]

Figure 5.1 Model development: (a) predicted strength of ASR-activated concrete; (b) ratio between CFRP-confined and unconfined concrete strengths; (c) empirical constants taken from optimized solutions; (d) adjustment factor

5.3 Design Proposal

An efficiency factor, ψ_{ASR}, is recommended when conducting a strengthening design for ASR-damaged concrete

$$\psi_{ASR} = \frac{\psi_{adj(withoutASR)}}{\psi_{adj(withASR)}} \tag{14}$$

It is important to state that Eq. 14 is intended to reflect the improved effectiveness of CFRP-confinement as the degree of ASR increased in the core concrete; accordingly, the factor (a relative comparison between the CFRP effects with and without ASR) is applicable to any existing confinement equation. For instance, the CFRP-confinement term in Eq. 10 can be multiplied by the ψ_{ASR} factor if used for upgrading ASR-damaged concrete members. Conforming to ASTM C1778 (ASTM 2016), four performance categories were established (Table 5.2) and linked with the results of the present test program, based on the level of strength reduction in the core concrete owing to the progression of ASR. The allocated performance levels agree with the configuration of general performance-based design approaches (Marsh and Stringer 2013). The calculated efficiency factors belonging to the individual replacement ratios are enumerated in Table 5.2 with minor adjustments.

Table 5.2 Performance-based ASR-efficiency factor for CFRP-confined concrete

Aggregate-reactivity (ASTM C1778)	Description of aggregate reactivity (ASTM C1778)	Present research		
		Replacement ratio	Potential strength reduction of concrete (f_c)	Ψ_{ASR} for confined concrete (f_{cc})
R0	Non-reactive	0%	<2%	1.00
R1	Moderately reactive	25%	≥2%,<10%	1.05
R2	Highly reactive	50%	≥10%,<15%	1.10
R3	Very highly reactive	75% to 100%	≥15%	1.15

6. SUMMARY AND CONCLUSIONS

This paper has discussed the behavior of concrete cylinders subjected to ASR with and without CFRP-confinement. To represent the variable amounts of ASR, reactive aggregates (rhyolite) substituted ordinary aggregates (granite) at a replacement ratio ranging from 0% to 100%, and the cylinders were conditioned as guided by ASTM C1260 (ASTM 2014a) in an NaOH solution. The time-dependent properties of the concrete and the solution were measured, and the progression of ASR through the concrete was optically assessed using a digital microscope. The structural responses of the plain and confined concrete specimens were examined with an emphasis on load-carrying capacity, toughness, and failure characteristics. An analytical model was developed to complement the experimental findings and to propose design recommendations. The following conclusions are drawn:

- The interaction between the NaOH solution and rhyolite resulted in accelerated ASR and altered the concrete mass, depending upon the aggregate replacement ratio. The potential of hydrogen (pH) in the solution decreased by up to 16% with the development of ASR, which was substantiated by the formation of hygroscopic gels.
- The stress-strain relationship of the plain concrete was generally linear until failure, while that of the confined concrete showed a bilinear transition when the core was substantially damaged by mechanical loading. Although the capacity of the confined concrete markedly improved relative to that of the plain concrete, over 370%, the ASR-damage in the core influenced the degree of the capacity enhancement.
- The average toughness of both plain and confined concrete cylinders without the NaOH exposure was maintained, irrespective of rhyolite amount; however, as the level of ASR elevated, an obvious decrease in toughness was noticed in conjunction with irreversible energy dissipation and degraded CFRP-concrete interaction.
- With an increase in ASR, the failure of the plain concrete became more complex with large spalling and multiple cracks, indicating a possible difference in bond between the rhyolite and granite aggregates with the cement binder. The integrity of the confined cylinders was a function of ASR: a transitional change in failure mode was observed between 50% and 75% replacement ratios, along with the explosive disintegration and shattering of the core concrete.
- The assessment of the present ACI 440.2R-17 equation revealed its limitation in predicting the confined strength of ASR-damaged concrete members. The efficiency factors resulting from the formulated analytical model are recommended to implement performance-based design for ASR-affected concrete confined with CFRP sheets.

7. REFERENCES

ACI. 1998. State-of-the-art report on alkali-aggregate reactivity (ACI 221.1R-98), American Concrete Institute, Farmington Hills, MI.

ACI. 2017. Guide for the design and construction of externally bonded FRP systems for strengthening concrete structures (ACI 440.2R-17), American Concrete Institute, Farmington Hills, MI.

ASTM. 2008. Standard test method for determination of length change of concrete due to alkali-silica reaction (ASTM C1293-08), American Society for Testing and Materials, West Conshohocken, PA.

ASTM. 2014a. Standard test method for potential alkali reactivity of aggregates (ASTM C1260-14), American Society for Testing and Materials, West Conshohocken, PA.

ASTM. 2014b. Standard test method for sieve analysis of fine and coarse aggregates (ASTM C136/C136M-14), American Society for Testing and Materials, West Conshohocken, PA.

ASTM. 2016. Standard guide for reducing the risk of deleterious alkali-aggregate reaction in concrete (ASTM C1778-16), American Society for Testing and Materials, West Conshohocken, PA.

ASTM. 2018. Standard specification for portland cement (ASTM C150/C150M-18), American Society for Testing and Materials, West Conshohocken, PA.

CSA. 2017. Design and construction of building structures with fibre-reinforced polymers (S806-12(R2017)), Canadian Standards Association, Toronto, ON, Canada.

Dyer, T. 2014. *Concrete Durability*, CRC Press, Boca Raton. FL.

Ferreira, T., and Rashband, W. 2012. *The ImageJ User Guide*, National Institute of Health, Bethesda, MD.

fib. 2001. *Externally bonded FRP reinforcement for RC structures* (Bulletin 14), International Federation for Structural Concrete, Lausanne, Switzerland.

Giaccio, G., Zerbino, R., Ponce, J.M., and Batic, O.R. 2008. “Mechanical behavior of concretes damaged by alkali-silica reaction,” *Cement and Concrete Research*, 38, 993-1004.

Glasser, F.P. 1992. Chemistry of the alkali-aggregate reaction, in *The Alkali Silica Reaction in Concrete*, Blackie Publishing, Glasgow, UK

Khan, M.A. 2010. *Bridge and highway structure rehabilitation and repair*, McGraw Hill, New York, NY.

Kubat, T., Al-Mahaidi, R., and Shayan, A. 2016. “CFRP confinement of circular columns affected by alkali-aggregate reaction,” *Construction and Building Materials*, 116, 98-109.

Lasdon, L.S., Fox, R.L., and Ratner, M.W. 1973. Nonlinear optimization using the General Reduced Gradient method, Technical Report AD-774723, Office of Naval Research, U.S. Department of Commerce, Springfield, VA.

Lindgard, J., Andic-Cakir, O., Fernandes, I., Ronning, T.F., and Thomas, M.D.A. 2012. "Alkali-silica reactions (ASR): literature review on parameters influencing laboratory performance testing," *Cement and Concrete Research*, 42, 223-243.

Marsh, M.L. and Stringer, S.J. 2013. "Performance-based seismic bridge design (NCHRP Synthesis 440)," Transportation Research Board, Washington, D.C.

Meddah, M.S., Zitouni, S., and Belaabes, S. 2010. "Effect of content and particle size distribution of coarse aggregate on the compressive strength of concrete," *Construction and Building Materials*, 24, 505-512.

Mehta, P.K. and Monteiro, P.J.M. 2014. *Concrete: Microstructure, Properties, and Materials*, McGraw Hill, New York, NY.

Mohamed, I., Ronel, S., and Curtil, L. 2006. "Influence of composite materials confinement on alkali-aggregate mechanical behaviour," *Materials and Structures*, 39, 479-490.

Neville, A.M. 1995. *Properties of Concrete, 4th edition*, Prentice Hall, Essex, UK.

Ng, T.F., and Beng, Y.E. 2007. "Potential alkali-silica reaction in aggregate of deformed granite," Geological Society of Malaysia, 53, 81-88.

Rajabipour, F., Giannini, E., Dunant, C., Ideker, J.H., and Thomas, M.D.A. 2015. "Alkali-silica reaction: current understanding of the reaction mechanisms and the knowledge gaps," *Cement and Concrete Research*, 76, 130-146.

Sanchez, L., Salva, P., Fournier, B., Jolin, M., Pouliot, N., and Hovington, A. 2012. "Evaluation of damage in the concrete elements of the viaduct Robert-Bourassa-Charest after nearly 50 years in service," 14th International Conference on Alkali-Aggregate Reactions in Concrete, 10 pp.

Saouma, V., and Perotti, L. 2006. "Constitutive model for alkali-aggregate reactions," *ACI Materials Journal*, 103(3), 194-202.

Sirivivatnanon, V., Mohamadi, J., and South, W. 2016. "Reliability of new Australian test methods in predicting alkali silica reaction of field concrete," *Construction and Building Materials*,126, 868-874.

Sjoberg, S. 1996. "Silica in aqueous environments," *Journal of Non-Crystalline Solids*, 196, 51-57.

Spencer, T.E., and Blaylock, A.J. 1997. "Alkali silica reaction in marine piles," *Concrete International*, 19(1), 59-62.

Thomas, M.D.A., Fournier, B., Folliard, K.J., and Resendez, Y.A. 2011. Alkali-silica reactivity field identification handbook, Report No. FHWA-HIF-12-022, Federal Highway Administration, Washington, D.C.

Thomas, M.D.A., Folliard, K.J., Fournier, B., Rivard, P., and Drimalas, T. 2013. Methods for evaluating and treating ASR-affected structures: results of field application and demonstration projects, Report No. FHWA-HIF-14-0002, Federal Highway Administration, Washington, D.C.

Torii, K., Sannoh, C., Kubo, Y., Ohashi, Y. 2004. "Serious damages of ASR affected RC bridge piers and their strengthening techniques," 12th International Conference on Alkali–Aggregate Reaction in Concrete, 1283-1288.

Ulm, F.-J., Coussy, O., Kefei, L., and Larive, C. 2000. "Thermo-chemo-mechanics of ASR expansion in concrete structures," *Journal of Engineering Mechanics*, 126(3), 233-242.